

# Localization of light in subradiant Dicke states: a mobility edge in the imaginary axis.

Giuseppe Luca Celardo

Benemérita Universidad Autónoma de Puebla, Instituto de Física, Apartado Postal J-48, Puebla 72570, Mexico

Mattia Angeli

International School for Advanced Studies (SISSA), Via Bonomea 265, I-34136 Trieste, Italy

Robin Kaiser

Université Côte d'Azur, CNRS, Institut de Physique de Nice, Valbonne F-06560, France

(Dated: May 28, 2018)

Anderson localization of light in three dimensions has challenged experimental and theoretical research for the last decades. Localization of light in cold atomic systems presents strong differences from the standard problem of localization since one needs to deal with an open quantum wave problem in presence of long range hopping which induces strong cooperative effects, such as super and subradiance. Contrary to common believe, we show that localization of light is possible in the dilute regime for subradiant states. Additional disorder in atomic transition frequencies leads to the emergence of a mobility edge in the immagibary axis, independent of the real energy. The existence of a critical lifetime above which subradiant Dicke states are localized appears as a general feature of scalar wave localization.

PACS numbers:

Strong localization, i.e. the absence of diffusion in a disordered sample, is an interference phenomenon proposed by Anderson in 1958 to explain the transition between a metallic and an insulating phase [1]. Since then, interferences in disordered systems have thus been at the focus of an ever increasing research community, ranging from condensed matter to acoustics, optics, and ultra-cold matter waves as well as quantum memories based on cold atoms [2–12]. Light has been an obvious candidate to study Anderson localization of non-interacting waves, which has triggered continuous efforts since the mid-80s [13–23]. Anderson localization of light in three dimensions however challenges this common believe. It has now been shown that past experiments on Anderson localization of light [16–18] do not provide a signature for the Anderson transition in three dimensions [19–23]. The mere existence of an Anderson phase transition for light is now being questioned [1, 2] and a possible solution implying a time-reversal symmetry breaking magnetic field has been proposed to overcome limitations due to near field coupling in the dense limit [26]. Here we propose a novel route towards localization of light in the dilute limit, where interatomic distances are large compared to the wavelength of the atomic transition.

In the standard Anderson localization problem, an excitation can tunnel to nearest-neighbor sites placed in a regular lattice with disordered energies (diagonal disorder) or disordered coupling (off-diagonal disorder). On the other side, light localization presents many features which strongly differs from Anderson localization problem: atoms have random positions in a three dimensional volume, leading to positional disorder and light induces complex long range hopping between the atomic sites, leading to cooperative effects such as Dicke sub- and superradiance [27–30]. Moreover the excitation can leave the system not only from the boundaries but from all atoms. This constitutes a major difference even w.r.t. open Anderson models, where the excitation can leave the system only from the boundaries [3]. Thus, the possi-

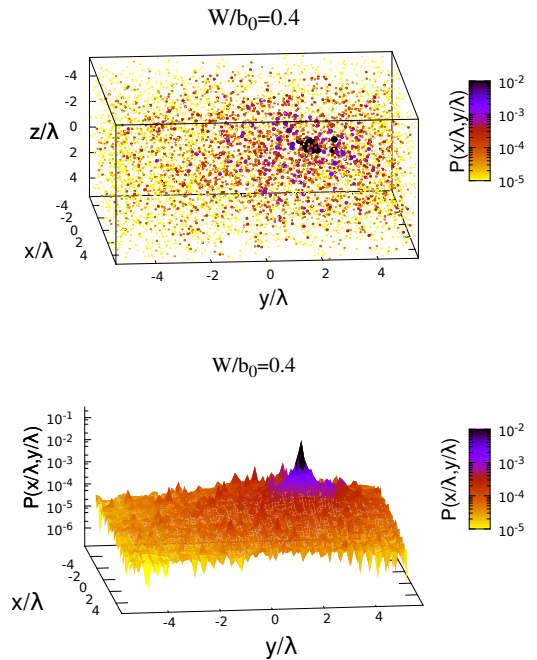


FIG. 1: (Color online) *Subradiant localized eigenstate*. Upper panel : Three dimensional representation of the eigenstate with  $\Gamma = 0.094$ ,  $E = 0.1$  and a participation ratio  $PR \approx 7$ . Here the radius representing each atom is proportional to its excitation probability  $|\Psi_j(r)|^2$ , also coded in color [50]. Lower panel: The same eigenstate projected on the  $x - y$  plane. Here  $N = 6400$ ,  $\rho\lambda^3 = 5$  corresponding to  $b_0 \approx 17.3$  and  $W/b_0 = 0.4$ .

bility to have a transition to localization in such systems is highly non-trivial, since we are dealing with an open quantum (wave) problem, where long range hopping and cooperative effects significantly change the transport properties. For

instance long range hopping is thought to destroy localization [32–34] for any amount of disorder. On the other side, cooperativity can affect the response of the system to disorder in a drastic way [5–7]: while superradiant states show robustness to disorder, in the subradiant subspace, long range interaction is effectively shielded [8, 9] and signature of localization can emerge [5, 6, 8]. Moreover in open systems, standard approaches to study localization such as the Thouless parameter should be applied with care [13], for this reason here we analyze directly the properties of the eigenmodes of the system.

Here we show that localization of subradiant Dicke states in clouds of cold atoms is possible in a regime previously thought impossible for localization. Indeed, we show that subradiant Dicke states [29, 41, 42] can be localized by additional diagonal disorder (additional random shifts of the atomic transition frequencies), on top of the positional disorder, in the dilute limit. In such a limit, near field dipole-dipole coupling can be neglected and the problem of localization of light can be described by scalar waves.

A general feature of the scalar wave localization described here is the emergence of a mobility edge in the imaginary axis, independent of the real energy. Since our system is open its eigenmodes have a finite lifetime. By mobility edge in the imaginary axis we mean the existence of a critical lifetime above which subradiant states are spatially localized with a participation ratio independent of the system size.

*The Model.*– In order to model a 3D cold atomic cloud, we consider  $N$  atoms randomly distributed inside a cube of volume  $V = L^3$ . Introducing the density  $\rho = N/L^3$  and the wavevector  $k_0 = 2\pi/\lambda$  we define the mean free path  $l = 1/\rho\sigma$ , where  $\sigma = 4\pi/k_0^2$  is the scattering cross section. Finally, we define the optical thickness,  $b_0$ , as the ratio between the system size  $L$  and the mean free path  $l$ :

$$b_0 = \frac{L}{l} = \rho \frac{4\pi}{k_0^2} \left(\frac{N}{\rho}\right)^{1/3}. \quad (1)$$

The optical thickness can be also related to the number of atoms which compete to decay in the same electromagnetic channel and can thus be understood as a measure of the cooperativity of the system [2, 27, 43]. Indeed since the number  $M$  of electromagnetic channels  $M \propto (L/\lambda)^2$ , we can write  $b_0 \propto N\lambda^2/L^2 \propto N/M$ .

We considered the single excitation effective Hamiltonian in the scalar approximation [44]. This approximation is appropriate in the dilute limit, where interatomic distances are larger than the optical wavelength, making near field terms decaying as  $1/r^3$  negligible.

The effective Hamiltonian which governs the interaction of the atoms with the electromagnetic field in this limit is characterized by long range hopping terms  $V_{i,j}$  decreasing as  $1/r_{ij}$  with the distance:

$$\mathcal{H} = \sum_{i=1}^N (E_i - i\frac{\Gamma_0}{2}) |i\rangle \langle i| + \frac{\Gamma_0}{2} \sum_{i \neq j}^N V_{i,j} |i\rangle \langle j| \quad (2)$$

where the state  $|i\rangle$  stand for the  $i$ -atom in the excited state and all the other atoms being in the ground state,  $V_{i,j} =$

$\frac{\exp(ik_0 r_{ij})}{k_0 r_{ij}}$  is the interaction between the atoms at distance  $r_{ij}$ .  $\Gamma_0$  is the natural decay width for a single atom. In the following energies and decay widths of the states will be expressed in units of  $\Gamma_0$ . Note that  $\mathcal{H}$  contains both real and imaginary parts which takes into account that the excitation is not conserved since it can leave the system by emission. Moreover  $1/(E - \mathcal{H})$  represents the propagator of an excitation inside the system, so that the eigenmodes and eigenvalues of  $\mathcal{H}$  determine the transport properties of the system [45].

The complex eigenvalues of this Hamiltonian describe the energy and line-widths of the eigenmodes of the system. We stress that even in the dilute limit  $\rho\lambda^3 \ll 1$  we can have cooperative behaviour in the large sample limit ( $L \gg \lambda$ ), provided that the cooperativity parameter  $b_0 \gg 1$ . In this regime cooperative effects such as single excitation sub- and superradiance become relevant [29, 41, 42]. Superradiant states are characterized by a decay width which is larger than the single atom natural width  $\Gamma_0$ , while subradiant states have a decay widths which are much smaller than the single atom decay width, as experimentally observed in dilute clouds of cold atoms [41].

In addition to the positional disorder of the atoms as studied previously [1, 2], we now introduce an additional random diagonal disorder term in the Hamiltonian,  $E_i$ , which shifts the excitation energy of the atoms. Experimentally in cold atomic clouds, such on-site disorder can be realized by applying a speckle field coupling the excited state to an auxiliary other excited state with convenient detuning, inducing thus random shifts of the atomic resonances without inducing dipole forces in the ground state. Following the approach of the Anderson model on lattice, we allow the site energies to fluctuate in the range of  $[-W/2, +W/2]$ , where  $W$  is the strength of disorder (in units of  $\Gamma_0$ ). Ensemble averaging thus includes different realizations of the random position of the atoms and of site disorder.

Within this model, we studied the eigenvalues as has been done in [1, 2] and the spatial profile of the eigenstates, which provide striking evidence when spatially localized eigenstates emerge [46]. In a more quantitative way, we also studied the participation ratio [47, 48],

$$PR = \left\langle \left| \sum_i |\langle i|\psi\rangle|^2 \right|^2 / \sum_i |\langle i|\psi\rangle|^4 \right\rangle, \quad (3)$$

of the eigenstates  $|\psi\rangle$  of the Hamiltonian Eq.(2), where  $\langle \dots \rangle$  stands for the ensemble average over different realizations of the static disorder and positional disorder [49]. Note that for the case of non-Hermitian Hamiltonians, the PR indicates the number of atoms over which the excitation is localized, provided it is found in the system [45]. The PR is a direct indicator of localization as for extended states, it increases proportionally to the system size,  $N$ , while, for localized states, it is independent of  $N$ . Often the problem of localization is analyzed also using the Thouless parameter [1, 2], nevertheless in many open systems this parameter can fail to signal localization transition [50].

*Localization Transition: critical disorder.*– A striking illustration of the existence of localized states is given in Fig. 1, where we represent a typical localized subradiant eigenstate.

The upper panel shows a 3D representation of the eigenstates, while the lower panel show the projection of  $|\psi(r)|^2$  on the  $x - y$  plane [50]. The addition of sufficient diagonal disorder, on top of the positional disorder, allows to obtain localized states, even in the dilute limit, where the Ioffe-Regel criterion (in absence of diagonal disorder) for localization ( $kl = 2\pi^2/\rho\lambda^3 \approx 4 > 1$  for the parameters of Fig. 1) is not fulfilled. We observe that the localized peak, shown in Fig. 1 b, come hand in hand with an extended tail, in agreement with Ref.s [5, 6]. The presence of an extended tail can strongly affect transport properties, for instance suppressing the exponential decay of transmission with the system size. Here we focus on the structure of the eigenmodes, leaving the analysis of the transport properties of subradiant localized states for a future work.

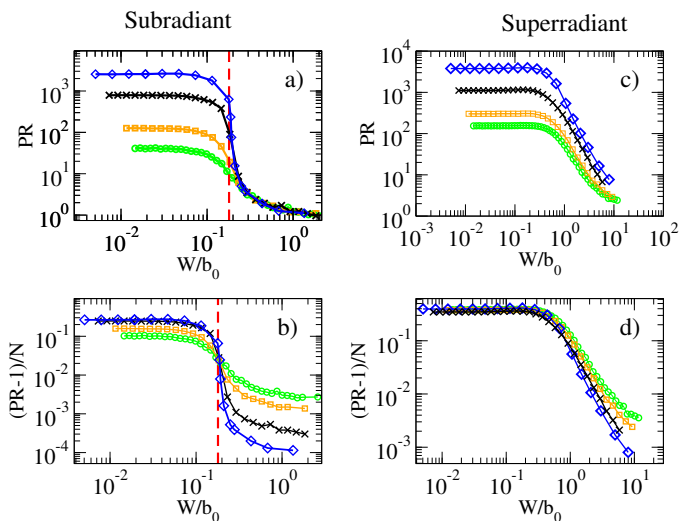


FIG. 2: (Color online) *Localization transition for subradiant states.* Average participation ratio for subradiant states (a,b) and superradiant states (c,d) as a function of the rescaled disorder  $W/b_0$ . The red dashed line indicates the critical disorder for localization Eq. (4). The values of  $PR$  are averaged over disorder and over eigenvalues in the interval  $-0.1 < E < 0.25$ .  $PR$  values are averaged over  $0.046 < \Gamma < 0.1$  for the subradiant states (a,b) and  $1 < \Gamma < 2.15$  for the superradiant states (c,d). Here the density is  $\rho\lambda^3 = 5$ . For each  $N$  we have different values of  $b_0 = 6.8$  ( $N = 400$ , green circles),  $8.6$  ( $N = 800$ , orange squares),  $13.7$  ( $N = 3200$ , black crosses),  $19.8$  ( $N = 9600$ , blue rombs).

In order to study the localization transition, we performed a systematic analysis [50] of the participation ratio vs the disorder strength  $W$  for different densities, system sizes and ranges of decay widths [51]. This analysis is summarized in Fig. 2, where we show the localization properties of the eigenmodes of the system for different system size at fixed density  $\rho\lambda^3 = 5$  and two different ranges of decay widths: a group of subradiant states ( $\Gamma < 1$ ) is shown in the left panels, while a group of superradiant states ( $\Gamma > 1$ ) is shown in the right panels. A clear signature of a transition to localization can be seen for the subradiant states when the disorder strength is rescaled by the optical thickness  $b_0$ . In Fig. 2(a), we show that below a critical  $W/b_0$ , the  $PR$  of the selected subradiant states

increases with the atom number, an indication of extended states. Above the a critical  $W/b_0$  however, the  $PR$  becomes independent of  $N$ , as expected from localized states. A more precise determination of the critical disorder can be obtained when looking at the normalized participation ratio as shown in Fig. 2(b) for the subradiant states: a universal crossing occurs which allows to determine  $W_{cr}/b_0$  for the localization transition. The behaviour of superradiant states (Fig. 2(c,d)) is in striking contrast to the behaviour of the subradiant states. Indeed the  $PR$  of the superradiant states is affected by disorder at much larger values of  $W/b_0$  and, most importantly, it does not become independent of the system size for any disorder considered (Fig. 2(c)).

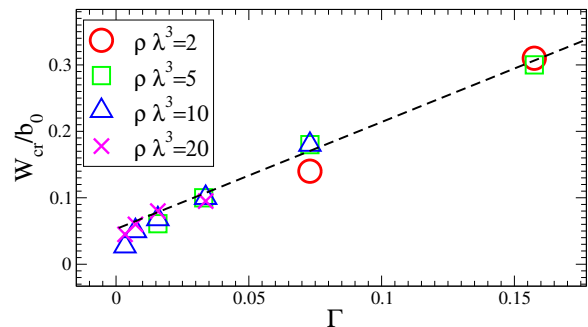


FIG. 3: (Color online) *Scaling of the critical disorder for localization.*  $W_{cr}$  rescaled by  $b_0$  is plotted vs the mean  $\Gamma$  for different densities. The black dashed line shows a linear fit, see Eq. (4).

By performing a similar analysis as in Fig. 2(b), for different densities and in all ranges of decay width, we determined the dependence of the critical disorder on  $b_0$ ,  $\Gamma$  and  $\rho$  [50]. We focused in a real energy window where the most subradiant states are, similarly to Ref. [1], even if our results apply to all the real energy range apart from the spectrum edges [50]. We also focused our analysis to the subradiant states, where a clear transition to localization has been observed. The result is illustrated in Fig. 3, where a linear dependence of  $W_{cr}/b_0$  vs  $\Gamma$  is clearly shown for sufficiently large values of  $\Gamma$ . The result can be summarized in the fitting formula of the critical disorder given by:

$$\frac{W_{cr}}{b_0} \sim 1.61 \Gamma + 0.053, \quad (4)$$

where both  $W_{cr}$  and  $\Gamma$  are in units of  $\Gamma_0$ . We also note that for high spatial densities and very small  $\Gamma$  a deviation from this law is observed, which lowers the values of the critical disorder needed to have a transition to localization. Even if a full understanding of Eq.(4) is very challenging, one can give the following heuristic explanation: (i) the energy width of the spectrum is proportional to  $b_0$  [2], allowing to use  $b_0$  as a measure of the coupling strength of excitation transition between the atoms. Similarly to the Anderson model the critical disorder is normalized by this coupling strength; (ii) the mean level spacing of the eigenmodes increases with the decay width, see Fig. (6) in [50], thus a larger disorder is needed to mix states with larger  $\Gamma$ . Thus Eq.(4) can be understood by

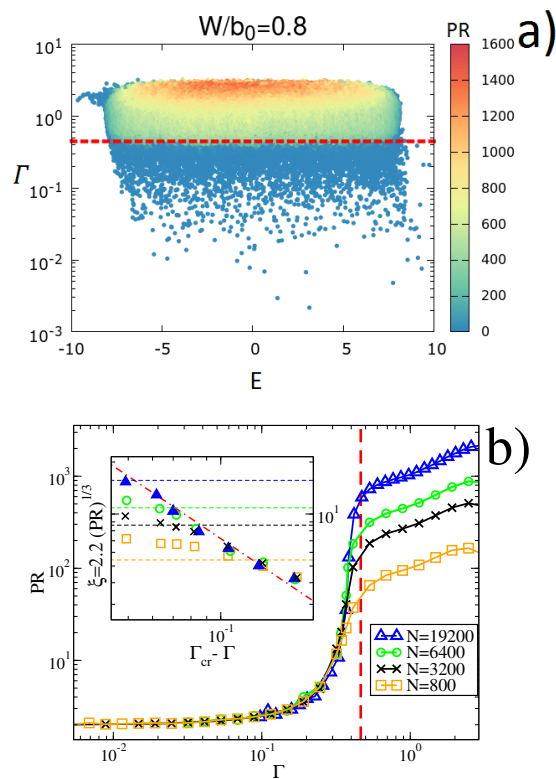


FIG. 4: (Color online) *Mobility edge in the imaginary axis*. Upper panel: Participation ratio of the eigenstates (see legend on the right) in the complex plane  $E, \Gamma$  of the eigenvalues of each state for  $N = 9600$ ,  $\rho\lambda^3 = 5$ ,  $b_0 \approx 19.8$  and  $W/b_0 = 0.8$ . The critical width for the transition to localization (Eq.(4)) is indicated by the red dashed horizontal line. Lower panel: Participation ratio as a function of the decay width of the eigenstates for  $W/b_0 = 0.8$ ,  $\rho\lambda^3 = 5$ . Here  $PR$  is averaged over the range  $-0.1 < E < 0.25$ . The vertical red dashed line indicates the critical width obtained from Eq. (4). In the inset we plot the estimated localization length  $\xi$  vs  $\Gamma_{cr} - \Gamma$ . The dashed-dot line shows  $(\Gamma_{cr} - \Gamma)^{1.2}$ . Horizontal lines show the size  $L$  for different values of  $N = 800, 3200, 6400, 19200$ .

a combination of the coupling strength determined by  $b_0$  and the  $\Gamma$  dependent mean energy spacing.

*Mobility edge in the imaginary axis*– From Eq. (4) one can determine the critical decay width for fixed  $b_0, N, \rho, W$  below which we have localized states. Indeed from Eq. (4) we can write for subradiant states ( $\Gamma < \Gamma_0$ ):  $\Gamma_{cr} \approx (W/b_0 - 0.053)/1.61$ . Fig.(4 a) shows the relevance of  $\Gamma_{cr}$ : for all values of the energy  $E$ , a sharp transition in the participa-

tion ratio is visible below  $\Gamma = \Gamma_{cr}$ , indicated by the dashed horizontal line, which corresponds to the appearance of a localized component on top a flat background. The appearance of a critical decay width is a novel feature of the transition to localization in open quantum wave systems in presence of cooperativity (sub- and superradiance). Interestingly it points to the existence of a “mobility edge” in the imaginary axis,  $\Gamma_{cr}$ , at which the  $PR$  of the subradiant states diverges, see Fig. 4 b. Remarkably the imaginary mobility edge is independent of  $E$  as shown in Fig. 4 a and further discussed in [50].

A preliminary study of how the localization length  $\xi$  diverges at the imaginary mobility edge is presented in the inset of Fig.(4 (b)). Since the  $PR$  gives the number of atoms over which the excitation is concentrated, for exponentially localized states in 3D, when  $PR \gg 1$ , we have  $PR \propto \rho\xi^3$ , allowing us to use the  $PR$  to estimate  $\xi$  close to the mobility edge. In the inset of Fig.(4 (b)) we plot  $\xi = A \times PR^{1/3}$  vs  $\Gamma_{cr} - \Gamma$  ( $A$  is a fitting constant) for different values of  $N$  and a fixed density. The dashed-dotted red line indicates  $\xi \propto (\Gamma_{cr} - \Gamma)^{-\nu}$  with  $\nu \approx 1.2$ , indicating a power law divergence of the localization length at the imaginary mobility edge. Even if the estimated critical exponent is close to that of the Anderson universality class, more analysis is needed to establish its value more accurately. In the inset of Fig.(4 b), we also plot the length of the sample  $L$  as horizontal lines. Note that both  $\xi$  and  $L$  are given in units of  $\lambda$ . By setting  $A = 2.2$  we find that the  $PR$  becomes roughly independent of  $N$  when  $\xi < L$ , for all the different  $N$  considered. This is consistent with our interpretation of  $\xi \propto (PR/\rho)^{1/3}$ .

*Conclusions.*– We considered a model [1, 2, 44] well suited to describe coherent multiple scattering of light in a dilute sample of two-level systems at low excitation level. The unique features emerging from our analysis is the existence of a “mobility edge” in the imaginary axis which is independent of energy. We demonstrate that disorder induces a divergence of the partition ratio at a finite critical decay width of the eigenmodes of the system, in analogy to the divergence of the participation ratio at a finite energy corresponding to the mobility edge of the Anderson model.

## Acknowledgments

We acknowledge stimulating discussions with R. Bachelard, A. Biella, F. Borgonovi, G. G. Giusteri and W. Guerin.

[1] P. W. Anderson, Phys. Rev. **109**, 1492 (1958).  
 [2] P. A. Lee and T. V. Ramakrishnan, Rev. Mod. Phys. **57**, 287 (1985).  
 [3] A. Lagendijk, B. A. van Tiggelen, Phys. Rep. **270**, 143 (1996).  
 [4] E. Akkermans and G. Montambaux, Mesoscopic physics of electrons and photons, Cambridge Univ. Press (2007).  
 [5] A. Lagendijk, B. van Tiggelen, D. S. Wiersma, Phys. Today **62**,

24 (2009).  
 [6] A. Aspect, M. Inguscio, Phys. Today **62**, 30 (2009).  
 [7] H. Hu, A. Strybulevych, J.H. Page, S.E. Skipetrov, B.A. van Tiggelen, Nature Phys. **4**, 945 (2008).  
 [8] J. Chabé et al., Phys. Rev. Lett. **101**, 255702 (2008).  
 [9] S. S. Kondov, W. R. McGehee, J. J. Zirber, B. DeMarco, Science **334**, 66 (2011).

- [10] F. Jendrzejewski et al., *Nature Phys.* **8**, 398 (2012).
- [11] G. Semeghini et al., *Nature Phys.* **11**, 554 (2015).
- [12] A. Asenjo-Garcia, M. Moreno-Cardoner, A. Albrecht, H. J. Kimble, D. E. Chang, arXiv:1703.03382v1.
- [13] S. John, *Phys. Rev. Lett.* **53**, 2169 (1984).
- [14] S. John, *Phys. Rev. Lett.* **58**, 2486 (1986).
- [15] P. W. Anderson, *Philos. Mag.* **B 52**, 505 (1985).
- [16] D. S. Wiersma, P. Bartolini, A. Lagendijk, R. Righini, *Nature* **390**, 671 (1997).
- [17] C. M. Aegerter, M. Störzer, G. Maret, *Europhys. Lett.* **75**, 562 (2006).
- [18] T. Sperling, W. Bührer, C.M. Aegerter, G. Maret, *Nature Photon.* **7**, 48 (2013).
- [19] F. Scheffold, R. Lenke, R. Tweer, G. Maret, *Nature* **398**, 206 (1999).
- [20] T. van der Beek, P. Barthelemy, P. M. Johnson, D. S. Wiersma, A. Lagendijk, *Phys. Rev. B* **85**, 115401 (2012).
- [21] F. Scheffold, D. Wiersma, *Nature Photon.* **7**, 934 (2013)
- [22] T. Sperling et al., *New. J. Phys.* **18**, 013039 (2016).
- [23] S. E. Skipetrov, J. H. Page, *New. J. Phys.* **18**, 021001 (2016).
- [24] S. E. Skipetrov, and I. M. Sokolov, *Phys. Rev. Lett.* **112**, 023905 (2014).
- [25] L. Bellando, A. Gero, E. Akkermans, and R. Kaiser, *Phys. Rev. A* **90**, 063822 (2014).
- [26] S.E. Skipetrov and I.M. Sokolov, *Phys. Rev. Lett.* **114**, 053902 (2015).
- [27] E. Akkermans, A. Gero, and R. Kaiser, *Phys. Rev. Lett.* **101**, 103602 (2008).
- [28] R. Kaiser, *J. Mod. Opt.* **56**, 2082 (2009).
- [29] T. Bienaime, N. Piovella, and R. Kaiser, *Phys. Rev. Lett.* **108**, 123602 (2012).
- [30] E. Akkermans and A. Gero, *Euro Phys. Lett.* **101**, 54003 (2013).
- [31] M. Weiss, J. A. Méndez-Bermúdez, and T. Kottos, *Phys. Rev. B* **73**, 045103 (2006).
- [32] L.S. Levitov, *Europhys. Lett.* **9**, 83 (1989).
- [33] L.S. Levitov, *Phys. Rev. Lett.* **64**, 547 (1990).
- [34] F. Evers and A.D. Mirlin, *Rev. Mod. Phys.* **80**, 1355 (2008).
- [35] G.L. Celardo, A. Biella, L. Kaplan, F. Borgonovi *Fortschr. Phys.* **61**, 250-260 (2013).
- [36] A. Biella, F. Borgonovi, R. Kaiser, G.L. Celardo, *EuroPhys. Lett.* **103**, 57009 (2013).
- [37] G.G. Giusteri, F. Mattiotti and G. L. Celardo, *Phys. Rev. B* **91**, 094301 (2015); G. L. Celardo, Giulio G. Giusteri, and F. Borgonovi, *Phys. Rev. B* **90**, 075113 (2014).
- [38] G. L. Celardo, R. Kaiser, and F. Borgonovi, *Phys. Rev. B* **94**, 144206 (2016).
- [39] L. F. Santos, F. Borgonovi and G. L. Celardo, *Phys. Rev. Lett.* **116**, 250402 (2016).
- [40] J. Wang and A. Z. Genack, *Nature* **471**, 435 (2011).
- [41] W. Guerin, M. O. Araújo, and R. Kaiser, *Phys. Rev. Lett.* **116**, 083601 (2016).
- [42] M. O. Araújo, I. Kresić, R. Kaiser, and W. Guerin *Phys. Rev. Lett.* **117**, 073002 (2016).
- [43] W. Guerin, M.-T. Rouabah, R. Kaiser, *J. Mod. Opt.* (2016): <http://dx.doi.org/10.1080/09500340.2016.1215564>.
- [44] S. Bux, E. Lucioni, H. Bender, T. Bienaime, K. Lauber, C. Stehle, C. Zimmermann, S. Slama, Ph. W. Courteille, N. Piovella and R. Kaiser, *J. Mod. Opt.* **57**, 2082 (2010).
- [45] V. V. Sokolov and V. G. Zelevinsky, *Ann. Phys. N.Y.L* **216**, 323 (1992); I. Rotter, *Rep. Prog. Phys.* **54**, 635 (1991); G. L. Celardo and L. Kaplan, *Phys. Rev. B* **79**, 155108 (2009); G. G. Giusteri, F. Mattiotti, and G. L. Celardo, *Phys. Rev. B* **91**, 094301 (2015).
- [46] C. E. Maximo, N. Piovella, Ph. W. Courteille, R. Kaiser, R. Bachelard, *Phys. Rev. A* **92**, 062702 (2015).
- [47] A Rodriguez, V A Malyshev and F. Dominguez-Adame, *J. Phys. A: Math. Gen.* **33**, L161 (2000).
- [48] A. Rodriguez, V.A. Malyshev, G. Sierra, M.A. Martin-Delgado, J. Rodriguez-Laguna, F. Dominguez-Adame, *Phys. Rev. Lett.* **90**, 027404 (2003).
- [49] The number of independent realizations over the random positions and energy shifts, was adjusted to ensure a total of at least  $\approx 10^6$  eigenvalues for each  $N, \rho$  and strengths of the disorder  $W$ .
- [50] see Supplementary Material.
- [51] Note that, since the atoms are randomly placed in a fixed volume, there will be a certain probability of two atoms being located very close to each other. This will induce pair-physics effects which should be neglected since here we are looking for collective effects (localization over many atomic states). We have avoided such pair-physics by a proper selection of the interval of complex energies as it has been done in previous works [1, 2]. Alternatively these effects can also be avoided by including an exclusion volume around each atom [41, 42].

**Supplementary material**  
**Localization of light in subradiant Dicke states: a mobility edge in the imaginary axis.**

**I. EXTENDED SUBRADIANT STATE**

Here we show an example of a typical extended subradiant state in presence of no diagonal disorder  $W/b_0 = 0$ , see Fig. (5). This figure should be compared with Fig. (1) of the main text where a typical localized subradiant state with  $W/b_0 = 0.4$  is shown. Comparing the two figures one can see that disorder in the transition frequencies of the atoms can induce localized states in the subradiant subspace. In both Fig. (5) of Supp. Mat. and Fig. (1) of the main text, in the upper panels each atom is shown by a small sphere. The probability  $|\Psi_j(r)|^2$  for the eigenstate to be on that atom is given by the color and the radius  $R$  of the sphere according to the relation  $R(r) = 1.5(|\Psi_j(r)|^2/|\Psi_j(r)|_{max}^2)^{2/7}$ , where  $|\Psi_j(r)|_{max}^2$  is the maximal probability for the case  $W/b_0 = 0.4$ . This normalization relation was chosen to improve visibility. In the lower panels the projection on the  $x-y$  plane of  $|\Psi_j(r)|^2$  on a grid of  $60 \times 60$  is shown. To improve the quality of the representation, each grid point has been averaged by the surrounding points, with a weighting inversely proportional to their distances squared.

In order to show that in absence of disorder most of the states of the system are indeed delocalized here we show a figure, Fig. (6), similar to Fig. (4) of the main text, but for a very small value of diagonal disorder  $W/b_0 = 0.005$ . In the upper panel of Fig. (6) we show that most of the states are delocalized, apart from few ones with a small  $PR$  which corresponds to pair physics [1, 2]. In the lower panel of Fig. (6) we show that, in absence of disorder, the  $PR$  of all the states (independently of the value of  $\Gamma$ ) increases with the system size in striking contrast with Fig. (4) lower panel of the main text.

**II. CRITICAL DISORDER IN THE DILUTE LIMIT**

Here we give a closer look at the localization transition extending the results shown in Fig. (2) of the main text to several decay width windows. In order to analyze the localization transition we will consider the participation ratio of the eigenmodes of the system, as we did in the main text. We note that the eigenfunctions of the non-Hermitian Hamiltonian represent the projection of the total eigenfunctions on the single excitation manifold of the atomic degrees of freedom. Thus the quantity  $|\psi_k|^2$  which is used to compute the PR represents the conditional probability to find the system on atom  $k$ , given that one quantum of excitation is stored in the system. The state  $|k\rangle$  is the state where the atom  $k$  is excited while all the other atoms are in the ground state. The PR thus measures over how many sites the excitation is distributed.

The eigenmodes of the system have been analyzed in different decay width windows for which  $\Gamma_{min} < \Gamma < \Gamma_{max}$ .

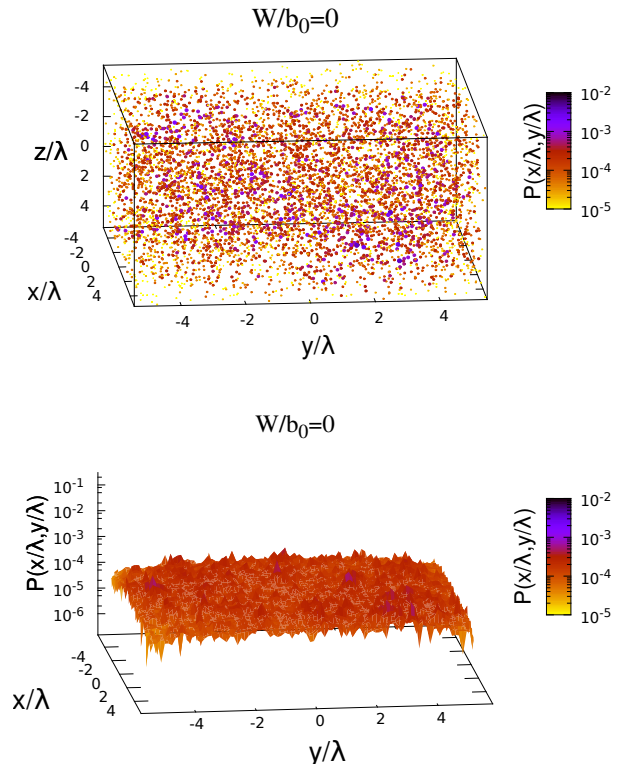


FIG. 5: (Color online) Representations of a typical extended subradiant state. Here is  $N = 6400, \rho\lambda^3 = 5$  so that  $b_0 \approx 17.3$  and  $W/b_0 = 0$ . For the state shown we have  $E = -0.0758, \Gamma = 0.05$ . The participation ratio  $PR$ , defined in Eq. (3) of the main text, of the state shown in this figure is  $PR = 1941$ .

In Fig. (7) we show the participation ratio  $PR$  of the states in several decay widths window as a function of the normalized disorder  $W/b_0$ , where  $b_0$  is the optical thickness defined in the main text. As one can see for subradiant states  $\Gamma < 1$  a transition to localization ( $PR$  becomes independent of  $N$ ) occurs above a critical value of the normalized disorder given by Eq. (4) in the main text, which we report here:  $W/b_0 \approx 1.61\Gamma + 0.053$ . Note that in Fig. (7) and Fig. (8) we used  $\Gamma = (\Gamma_{max} - \Gamma_{min})/2$  to obtain the critical disorder. On the other side, superradiant states  $\Gamma > 1$  do not show any transition to localization in the range of disorder considered here, so that our estimate of the critical disorder does not apply for them.

In Fig. (8) the normalized participation ratio is plotted versus the normalized disorder for the same decay width windows shown in Fig. (7). As one can see for the subradiant states a crossing occurs at a specific value of  $W/b_0$ . Such crossing allowed us to extract the critical normalized disorder which has been fitted with Eq. (4) in the main text. The results presented here clearly show the dependence of the critical disorder on the decay width and the fact that a localization transition is a generic property of subradiant states. Note that the data shown in Fig.s (7) and (8) refer to a density  $\rho\lambda^3 = 5$ , but our analysis has been extended also to other densities, see

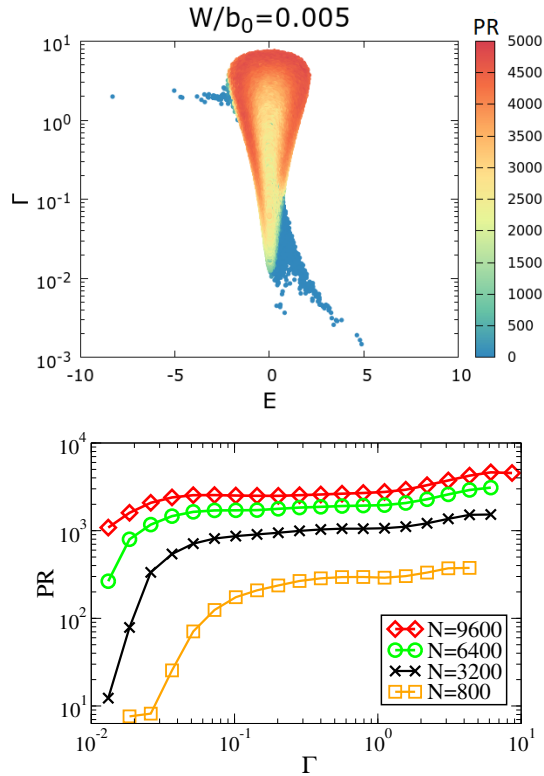


FIG. 6: (Color online) *Extended subradiant states*. Upper panel: Participation ratio of the eigenstates (see legend on the right) in the complex plane  $E, \Gamma$  for  $N = 9600$ ,  $\rho\lambda^3 = 5$ ,  $b_0 \approx 19.8$  and  $W/b_0 = 0.005$ . Lower panel: Participation ratio as a function of the decay width of the eigenstates for  $W/b_0 = 0.005$ ,  $\rho\lambda^3 = 5$ . Here  $PR$  is averaged over the range  $-0.1 < E < 0.25$ .

Fig. (3) in the main text, where the critical disorders extracted from the crossing of the normalized  $PR$  vs  $W/b_0$  for different densities and different decay windows is shown.

### III. ON THE NATURE OF THE IMAGINARY MOBILITY EDGE

Usually in open Anderson models [3], the excitation can escape the system only from the boundaries, so that the decay widths are proportional to the probability of a state to be on the boundaries. As a consequence of this, most of the localized states also have very long lifetimes (similar to subradiant states), since their probability to be on the boundaries is exponentially small. On the other side, the model studied here, see also Ref.s [4], strongly differs from the previously studied models of localization in open systems, since in our case the excitation can escape from any site and not only from the boundaries. For instance in our model a fully localized state on one site has a decay width equal to  $\Gamma_0$ , independent of the system size, which is not exponentially small. Let us consider a 3D cubic Anderson model with leads connected to one of its side as in [3]. Let us assume that the disorder is such to create a mobility edge at energy  $E_c$ . Clearly the decay width

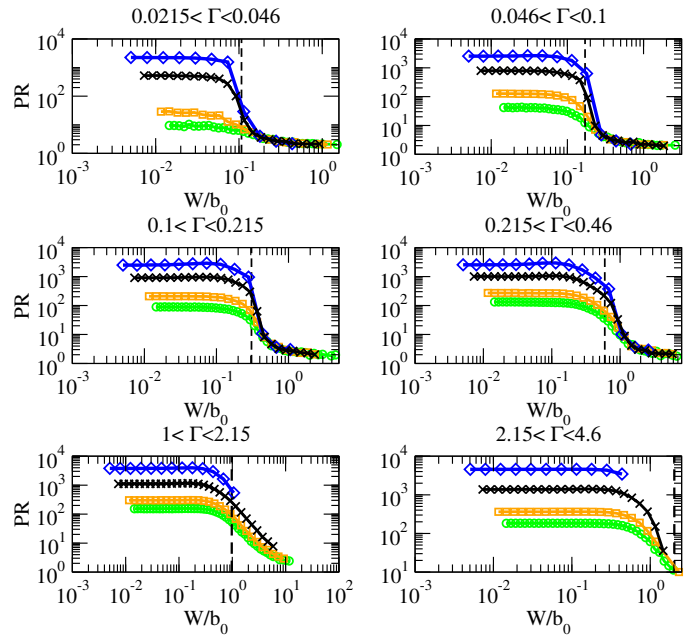


FIG. 7: (Color online) *Localization transition for subradiant states*. Average participation ratio of the states in different decay width windows (see figure) as a function of the rescaled disorder  $W/b_0$ . The vertical dashed black line indicates the critical disorder, see Eq. (4) of the main text, for localization for the subradiant states. Note that for superradiant states  $\Gamma > 1$  there is no transition to localization and our estimate of the critical disorder does not apply. The values of  $PR$  are averaged over disorder and over eigenvalues in the interval  $-0.1 < E < 0.25$ . Here the density is  $\rho\lambda^3 = 5$ . Note that for each  $N$  we have different values of  $b_0 = 6.8$  ( $N = 400$ , green circles),  $8.6$  ( $N = 800$ , orange squares),  $13.7$  ( $N = 3200$ , black crosses),  $19.8$  ( $N = 9600$ , blue rombs).

of the states will be very small for  $E < E_c$ , while they will be large for energy  $E > E_c$ , and correspondingly a mobility edge could also be found in the imaginary axis if one plot the participation ratio  $PR$  vs the decay widths. But in this case to use  $E$  or  $\Gamma$  is just a different way to label the states. On the other side our mobility edge has a completely different nature since it is independent of the real energy of the states, but it only depends on their imaginary energy. This is further shown in Fig. (9). In Fig.(9 upper panel), the  $PR$  for all eigenvalues is shown for a different value of disorder with respect to Fig. (4a) in the main text. Also in this case, for all values of the energy  $E$  (apart from the spectrum edges), a sharp transition in the participation ratio is visible for a given value of  $\Gamma = \Gamma_{cr}$ , indicated by the dashed horizontal line. In Fig.(9 lower panel), we consider the same case of Fig. (4b) in the main text, but now we analyze a different energy interval. As one can see, the same critical width signals the transition to localization in both cases, showing that the imaginary mobility edge is independent of energy. Also the power law divergence seems to be independent of the energy, see inset of Fig. (9 lower panel) and compare it with the inset of Fig. (4b) in the main text.

We note that the dependence of the  $PR$  on the lifetime of the subradiant eigenmodes is a novel feature, which has not been captured by the toy model of Ref.s [5, 6]. Indeed, in

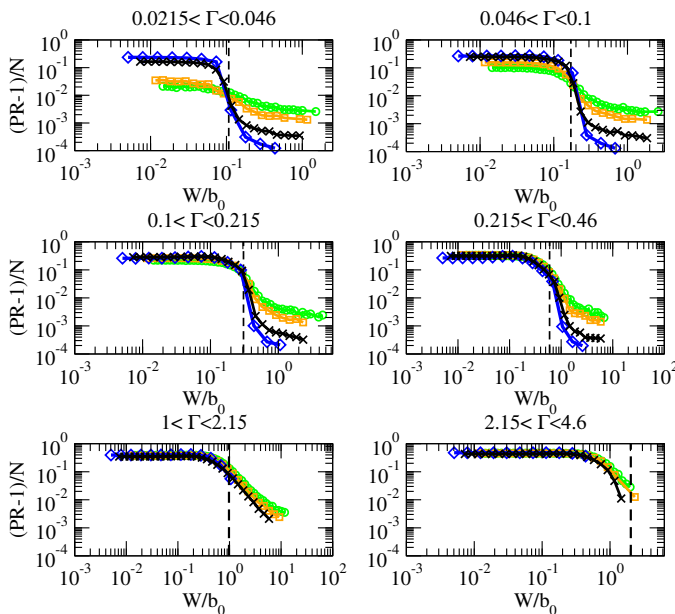


FIG. 8: (Color online) *Localization transition for subradiant states.* Average normalized participation ratio of the states in different decay width windows (see figure) as a function of the rescaled disorder  $W/b_0$ . The vertical dashed black line indicates the critical disorder for localization, Eq. (4) in the main text, for the subradiant states. The values of  $PR$  are averaged over disorder and over eigenvalues in the interval  $-0.1 < E < 0.25$ . Here the density is  $\rho\lambda^3 = 5$ . Note that for each  $N$  we have different values of  $b_0 = 6.8$  ( $N = 400$ , green circles),  $8.6$  ( $N = 800$ , orange squares),  $13.7$  ( $N = 3200$ , black crosses),  $19.8$  ( $N = 9600$ , blue rombs).

the open 1D and 3D Anderson model analyzed in Ref. [5, 6], the sub- and superradiant modes were segregated in two regions, whereas in the present case, no gap between sub- and superradiant modes exists. For the situation considered in this letter, the increase of PR with  $\Gamma$  can be explained by the increase of the mean level spacing of the eigenvalues with  $\Gamma$ , see Fig. (10). Note that in Fig. (10) we compute the mean level spacing in the complex plane of the complex eigenvalues of the system. Indeed perturbation theory in the case of non-Hermitian Hamiltonian shows that it is the distance in the complex plane which determines the strength of perturbations [7]. Moreover we checked that also the mean level spacing in the real axis increases with the decay width. The increase of the mean level spacing with the decay width is due to the fact that superradiant states have a stronger coupling to the photon field, so that their energy spreads much more than subradiant states, which are partially shielded from the interaction [8]. Thus for a fixed amount of disorder, the states with lower  $\Gamma$  are more easily mixed by disorder than the states with a larger  $\Gamma$ . This can also explain the dependence of the critical disorder on  $\Gamma$  given in Eq. (4) of the main text. We also note that a highly non-uniform mean level spacing is typical for systems with long range interactions. For instance even a finite energy gap can be induced in such systems [8]. Localization even in presence of long range interaction has been discussed for subradiant states in [5, 6] and in general, in

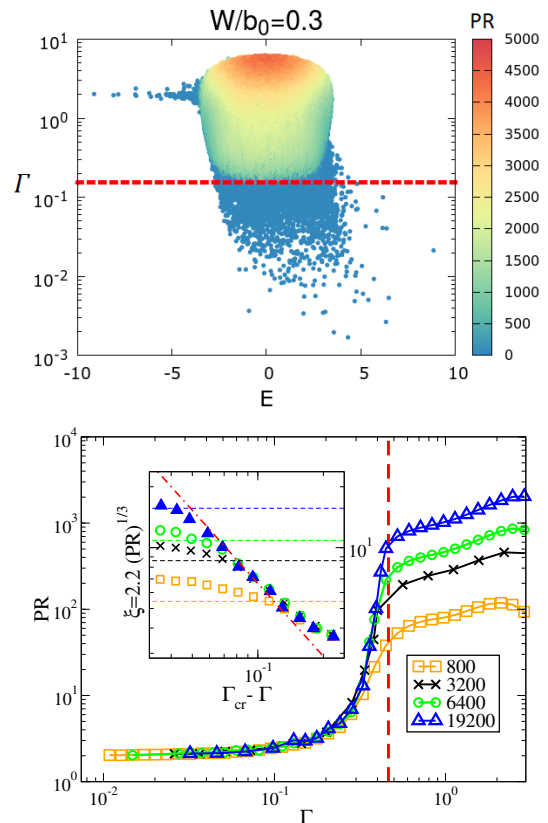


FIG. 9: (Color online) *Mobility edge in the imaginary axis.* Upper panel: Participation ratio of the eigenstates (see legend on the right) in the complex plane  $E, \Gamma$  of the eigenvalues of each state for  $N = 9600$ ,  $\rho\lambda^3 = 5$ ,  $b_0 \approx 19.8$  and  $W/b_0 = 0.3$ . The critical width of the resonance for the transition to localization (Eq. (4) in main text) is indicated by the red horizontal line. Lower panel: Participation ratio as a function of the decay width of the eigenstates for  $W/b_0 = 0.8$ ,  $\rho\lambda^3 = 5$ . Here  $PR$  is averaged over the range  $2 < E < 3$ . The vertical red dashed line indicates the critical width obtained from Eq. (4) in the main text. In the inset we plot the estimated localization length  $\xi$  vs  $\Gamma_{cr} - \Gamma$ . The dashed-dot line shows  $(\Gamma_{cr} - \Gamma)^{1.2}$ . Horizontal lines show the size  $L$  for different values of  $N = 800, 3200, 6400, 19200$ .

the framework of a shielding effect in [8, 9] and more recently in [10].

Finally we note that in the closed Anderson 3D model, the PR diverges at a finite energy corresponding to the mobility edge. In our case, the PR diverges at a finite decay width (corresponding to the imaginary part of the complex eigenvalues of the system), thus we use the term mobility edge in the imaginary axis in analogy with the localization transition in closed systems which occurs along the real axis. In the case of a closed systems, such as the standard Anderson model, the behavior of the PR reflects the transport properties of a system in a direct way: when the PR increases with the system size, transmission will be diffusive or ballistic, while if the PR is independent of the system size, transmission is exponentially suppressed with the system size due to localization. In the case of open systems, described by a non-Hermitian Hamil-

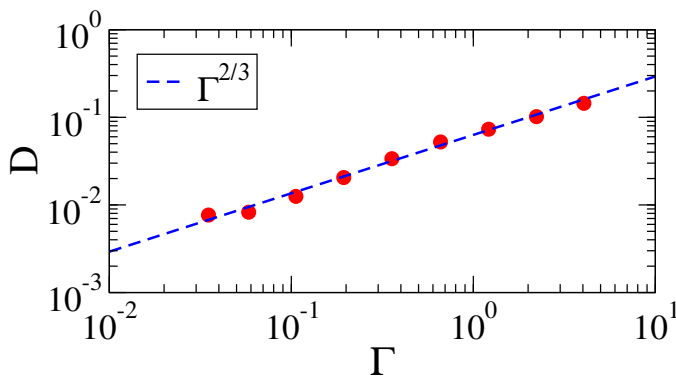


FIG. 10: (Color online) Increase of the mean level spacing with the widths. The mean level spacing in the complex plane  $D$  is plotted vs the decay widths  $\Gamma$  (red circle) for the case  $N = 3200$ ,  $\rho = 5$  and  $W = 0$ . The mean level spacing has been computed by counting the number of complex eigenvalues per unit area in the complex plane for  $-0.1 < E < 0.25$  and different ranges of  $\Gamma$ . The mean level spacing  $D$  has been obtained by taking the square root of the inverse density of complex eigenvalues. Note that an increase of the mean level spacing is observed even if one compute the distance in the real energy axis of the complex eigenvalues.

tonian, the PR has a more indirect link to transport properties and we do not aim to discuss this link in this manuscript. Nevertheless, also in this case,  $1/(E - H)$  is the propagator for the excitation in the system. For this reason, a change in the structure of the eigenmodes of  $H$  as signaled by the PR represents a real physical change in the way excitations propagate through the system.

#### IV. LOCALIZATION AND DENSITY

Here we compare our analysis of the localization properties of the scalar model for cold atomic clouds with the results obtained in previous works, which used a resonance overlap or Thouless parameter as indicator for localization [1, 2]. As reported in Ref. [1, 2] the analysis of the Thouless parameter in the scalar model predicts Anderson localization at high densities in cold atomic clouds (mainly due to the positional disorder) even in the absence of diagonal disorder. In Fig. 11 the mean participation ratio  $PR$ , defined in Eq. (3) of the main text, is shown as a function of the density of a group of subradiant states at a fixed and negligible disorder (considerably lower than  $W_{cr}$ , see Eq. (4) of the main text). When the densities are large enough ( $\rho\lambda^3 > 24$ ) these states are indeed localized, above a critical density which is in excellent agreement with Ref. [1, 2]. In order to avoid such a high density transition, we kept the densities analyzed in the main text at values well below that critical value. Note however that at large densities the scalar model is not a good description of atom-light coupling and a more refined models, including polarization and near field dipole-dipole coupling, does not show signatures of localization in the dense limit [1, 2]. On the other side, the localization transition observed in the dilute limit in the main text is experimentally relevant. As a final remark,

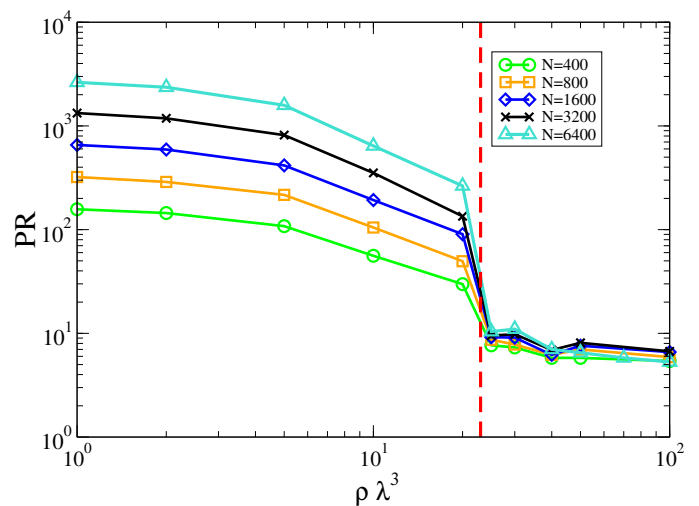


FIG. 11: (Color online) Average participation ratio of a group of subradiant states with  $0.01 < \Gamma < 1$  as a function of the density  $\rho\lambda^3$  at fixed very small disorder  $W \approx 0.1$ . The transition to localization occur at  $\rho \approx 24$  (red dashed line), in agreement with the results in Ref. [1, 2].

let us note that the fact the analysis of the Thouless parameter done in Ref. [1, 2] is in agreement with our analysis is a surprising result. Indeed, as it will be clear from the discussion in the next section, in open quantum wave problems, the Thouless parameter can fail to signal localization transition.

#### V. LOCALIZATION TRANSITION AND THE THOULESS PARAMETER

In the main text we gave evidence of a transition to localization occurring as the parameter  $W/b_0$  crosses a critical value. We remind that  $W$  is the strength of the disorder and  $b_0$  is the optical thickness defined in Eq. (1) of the main text. The transition to localization has been analyzed by looking at a direct measure of localization: the participation ratio  $PR$ , defined in Eq. (3) of the main text. It was shown that above a critical value of  $W/b_0$  the PR of the subradiant states becomes independent of the system size, if the density is kept fixed, see Fig. (2a,b) of the main text. This is a clear signature of localized eigenstates.

Often the problem of localization is analyzed using the Thouless parameter (or conductance)  $g$  [11, 12]. Roughly  $g$  can be defined as the ratio of the average decay width over the mean level spacing and it measures the overlapping between the eigenmodes of the system. In the localized regime we have that  $g < 1$  and it should decrease with the systems size, on the other side, in the extended regime we have that  $g > 1$  and it increases as the system size.

The  $g$  parameter can be defined, see in Ref. [1, 2], as:

$$g = \left\langle \frac{(2/\Gamma)^{-1}}{\Delta E} \right\rangle \quad (5)$$

where  $1/\Delta E$  is the inverse nearest-neighbor average level

spacing, proportional to the Heisenberg time, and  $\overline{2/\Gamma}$  is the average of the inverse modal leakage rate, which is proportional to the Thouless time. Here  $\overline{\dots}$  denotes the average over the eigenstates in a given energy window for a single realization of positional disorder and  $\langle \dots \rangle$  denotes the average over all configurations. Even if the  $g$  parameter is able to capture the localization transition which occurs at high density, see previous Section, care is needed in using the Thouless parameter in open systems, when the leakage of the excitation does not occur only from the boundaries. Indeed we verified that the use of  $g$  does thus not signal any transition to localization as a function of  $W/b_0$ , even if we know it occurs from the study of the participation ratio, see Fig. (2a,b) in the main text.

To further show that the  $g$  parameter fails to signal the localization transition driven by disorder, we computed the Thouless parameter while increasing the value of the system size, keeping the density  $\rho\lambda^3 = 5$  constant. The results of our analysis are shown in Fig. (12). As one can see the  $g$  parameter increases with the system size for all the values of  $W$ , corresponding to a scaling function  $\beta = \frac{\partial \ln(g)}{\partial \ln(L)}$  [12] remaining positive for all values of  $W$ .

The fact that the  $g$  parameter does not capture the diagonal disorder induced transition discussed in this paper but does

capture the high density induced transition to localization requires further investigation. We note that in contrast to the study of electron transport and numerical studies of Anderson localization on lattices, here we are in presence of a system where coupling to the outgoing modes does not only arise from atoms at the boundary of the system. In the coupled dipole model, the outgoing electromagnetic field is obtained by a sum over the fields scattered by all dipoles, not only those located at the boundary. As previously studied in [3], the presence of leads connecting the open channels to sites not restrained to the boundary, can strongly affect the distribution of lifetimes of the eigenmodes and thus the  $g$  parameter. In conclusion we are not claiming that a properly defined Thouless parameter cannot work in our case, but only that the common definition of the Thouless parameter used in literature can be misleading in our case. Indeed in presence of absorption or other sources of leakage the decay width of the states should be properly redefined in order to take into account only the leakage from the boundaries, see discussion in Ref. [13]. This redefinition is not simple in our model due to the fact that the decay widths are the result of the interaction of many atoms.

- 
- [1] S. E. Skipetrov, and I. M. Sokolov, Phys. Rev. Lett. **112**, 023905 (2014).
- [2] L. Bellando, A. Gero, E. Akkermans, and R. Kaiser, Phys. Rev. A **90**, 063822 (2014).
- [3] M. Weiss, J. A. Mendez-Bermudez, T. Kottos, Resonance width distribution for high-dimensional random media, Phys. Rev. B **73**, 045103 (2006).
- [4] G.L. Celardo, A. Biella, L. Kaplan, F. Borgonovi Fortschr. Phys. **61**, 250-260 (2013); A. Biella, F. Borgonovi, R. Kaiser, G.L. Celardo, EuroPhys. Lett. **103**, 57009 (2013).
- [5] G.L. Celardo, A. Biella, L. Kaplan, F. Borgonovi Fortschr. Phys. **61**, 250-260 (2013).
- [6] A. Biella, F. Borgonovi, R. Kaiser, G.L. Celardo, EuroPhys. Lett. **103**, 57009 (2013).
- [7] G. L. Celardo, Giulio G. Giusteri, and F. Borgonovi, Phys. Rev. B **90**, 075113 (2014).
- [8] G. L. Celardo, R. Kaiser, and F. Borgonovi, Phys. Rev. B **94**, 144206 (2016).
- [9] L. F. Santos, F. Borgonovi and G. L. Celardo, Phys. Rev. Lett. **116**, 250402 (2016).
- [10] X. Deng, V. E. Kravtsov, G. V. Shlyapnikov, L. Santos, arXiv:1706.04088.
- [11] D. J. Thouless, Phys. Rev. Lett. **39**, 1167 (1977)
- [12] E. Abrahams, P. W. Anderson, D. C. Licciardello, and T. V. Ramakrishnan, Phys. Rev. Lett. **42**, 673 (1979)
- [13] J. Wang and A. Z. Genack, Nature **471**, 435 (2011).

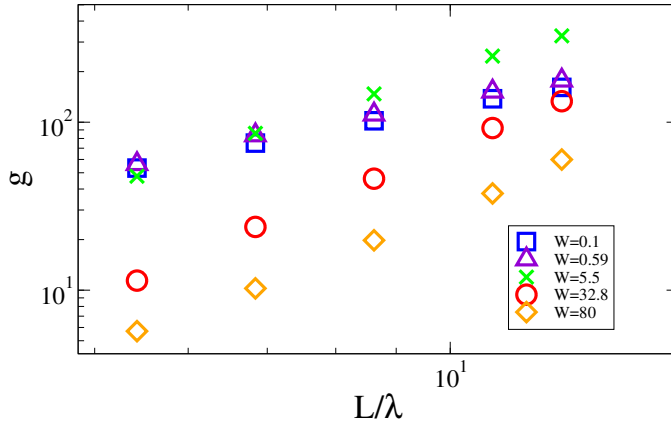


FIG. 12: (Color online) Thouless parameter as a function of the rescaled length of the system  $L/\lambda$  and different disorder strength (see figure) keeping the density  $\rho\lambda^3 = 5$  constant. Note that to keep the density constant for each value of  $L/\lambda$  we have a different value of  $N$  and a corresponding value of  $b_0 = 8.6$  ( $N = 800$ ),  $b_0 = 10.89$  ( $N = 1600$ ),  $b_0 = 13.7$  ( $N = 3200$ ),  $b_0 = 17.29$  ( $N = 6400$ ),  $b_0 = 19.8$  ( $N = 9600$ ). The average was done over disorder and different eigenvalues in the interval  $-0.1 < E < 0.25$  (the real part of the eigenvalues) and with no restrictions on  $\Gamma$ .